1.D.2 *Nuclear Physics* A253 (1975) 231–252;

ASYMMETRIC ROTOR MODEL FOR DECOUPLED BANDS IN TRANSITIONAL ODD-MASS NUCLEI

H. TOKI

Institut für Kernphysik der Kernforschungsanlage Jülich, D-517 Jülich, West Germany

and

AMAND FAESSLER

Institut für Kernphysik der Kernforschungsanlage Jülich, D-517 Jülich, West Germany

and

University of Bonn, D-53 Bonn, West Germany

Received 22 May 1975
(Revised 27 June 1975)

Abstract: The high-spin states in transitional odd-mass nuclei are studied in terms of an odd quasi-particle coupled to an asymmetric rotor with a variable moment of inertia (VMI). In order to take into account the VMI, the basis states are expanded in terms of the core eigenfunctions. Excitation energies, quadrupole moments, magnetic moments, B(E2) values and B(M1) values are calculated and compared with the experimental data for nuclei in Au and La regions. On comparison with other descriptions it is found that the treatment with VMI provides a more satisfactory explanation of the data.

1. Introduction

Recently a large number of decoupled bands in transitional odd-mass nuclei has been measured using (heavy ion, xn) reactions [1]). The rotational bands built on larger single particle angular momentum states $|j\rangle$ show a spin sequence $j, j+2, j+4, \ldots$ and an energy spacing almost equal to that of the adjacent even nuclei for the angular momenta $0^+, 2^+, 4^+, \ldots$. An explanation for these decoupled bands has been given by Stephens *et al.* [2]) on the basis of Coriolis decoupling according to which the angular momentum of the odd particle tends to be parallel to that of the core. More recently Meyer-ter-Vehn and coworkers [3]) have calculated the excitation energies of the nuclei in the Au region in terms of an odd particle coupled to an asymmetric rotor. In their work the necessity of introducing the γ-deformation is stressed. The results of these calculations are not satisfactory in the sense that though the ordering of the levels is reproduced the excitation energies of especially the high-spin levels are always higher than those given by experiments. However, this is quite expected due to the following fact. It is well known that in the transitional regions the rigid rotor model does not give satisfactory excitation energies. (For example, if we fix in an even-mass nucleus the moment of inertia from the excitation energy of

the first 2^+ state, the other excitation energies are higher than those of experiments.) Inclusion of the softness of the core is required for any quantitative agreement with the excitation energies of even-mass nuclei. We adopt this point of view in the present paper and give a detailed account of our study of the high-spin states in transitional odd-mass nuclei (Au and La regions) in terms of an odd quasi-particle coupled to an asymmetric rotor with a variable moment of inertia (VMI). We treat the softness of the core by expanding the basis states in terms of the eigenfunctions of the angular momentum of the core. In this basis the variable moment of inertia [4]) (VMI) of the core is diagonal. In our calculations we also include the pairing effect which is important for the nuclei far off from the magic numbers. The parameters of the Hamiltonian which are adopted in every pair of even- and odd-mass nuclei are: the moment of inertia θ_0 and softness parameter C of the VMI model in the even-mass nucleus, the deformation parameter γ in the even- and/or odd-mass nucleus and the Fermi energy λ in the odd nucleus. The parameters are adjusted by minimizing the χ^2 using the Simplex method [5]). We calculate the excitation energies, B(E2) values and B(M1) values for Ir, Au and Hg isotopes in the $A = 190$ region and for the nuclei ^{133}La and ^{135}Pr. On comparison with other calculations it is found that the treatment with VMI provides a more satisfactory description of the data.

In sect. 2 the nuclear model is introduced and the relevant formula presented. In sect. 3 the expressions for the transition probabilities B(E2) and B(M1) are given. The results of this model are compared with the experimental data in sect. 4. Sect. 5 contains a discussion and a summary of the model and of the conclusions of this work.

2. The nuclear model

The Hamiltonian of an odd-particle system in our model is written as

$$H = \sum_{n=1}^{3} \frac{R_n^2}{2\theta_{nR}} - k\{\cos\gamma Y_{20} + \sqrt{\tfrac{1}{2}}\sin\gamma(Y_{22} + Y_{2-2})\} - G\sum_{ab>0} c_a^+ c_{\bar{a}}^+ c_{\bar{b}}\, c_b, \quad (1)$$

where $Y_{\lambda\mu}$ are spherical harmonics, R_n are the core angular momenta, G is the pairing strength and c_a^+ is the creation operator of the state $|a\rangle$, whereas $|\bar{a}\rangle$ means the time-reversed state. In eq. (1) the particle deformation coupling strength k is taken to be $k = (\frac{4}{5}\pi)^{\frac{1}{2}}\, 206\, A^{-\frac{1}{3}}\, \beta$ MeV [ref. [3])]. This gives the empirical single particle spacings at $\gamma = 0$ for a nucleus with mass A. The moment of inertia θ_{nR} is given by $\theta_{nR} = \frac{4}{3}\theta_{0R}\sin^2(\gamma - \frac{2}{3}\pi n)$ for the intrinsic axes $n = 1, 2, 3$. The Bohr-Mottelson parameters β and γ are the symmetric and asymmetric quadrupole deformations, respectively. The moment of inertia parameter θ_{0R} depends according to the VMI model [4]) on the angular momentum of the core [see eqs. (13) to (15)]. In order to get the single particle states $a_i^+|0\rangle$ we diagonalize the single particle Hamiltonian given by the second term in eq. (1). They are expressed by the creation operators

$c^+_{j\Omega}$ in a spherical basis

$$a^+_i = \sum_{\Omega} W^i_{\Omega} c^+_{j\Omega}, \tag{2}$$

where we take the phase convention of W^i_{Ω} as real, and the angular momentum projection Ω satisfies mod $(\Omega - \frac{1}{2}, 2) = 0$. In eq. (2) and in all this work we restrict the discussion to a single j-shell (for example: $i_{13/2}$, $h_{9/2}$, $h_{11/2}$), which is indicated for every nucleus in the figure captions. Therefore the sum in eqs. (2) and (3) runs only over the single particle angular momentum projection to the intrinsic z-axis. The creation operator of the time-reversed state of $|i\rangle$ is written as

$$a^+_{\bar{i}} = \sum_{\Omega} W^i_{\Omega} c^+_{j\bar{\Omega}} = \sum_{\Omega} W^i_{\Omega} (-)^{l+j-\Omega} c^+_{j-\Omega}, \tag{3}$$

where we take the time-reversed phase as $(-)^{l+j-\Omega}$. The pairing Hamiltonian is treated by the BCS method. With this the single particle part (together with the deformation term proportional to k), including the pairing term of the Hamiltonian (1), can be written as

$$H_{\text{s.p.}} = \sum_i E_i \alpha^+_i \alpha_i, \tag{4}$$

with

$$\alpha^+_i = u_i a^+_i - v_i a_{\bar{i}},$$

where α^+_i and α_i are the quasi-particle creation and annihilation operators of a deformed single particle state. The quasi-particle energy E_i is given as $E_i = \sqrt{(\varepsilon_i - \lambda)^2 + \Delta^2}$. Here α_i are the deformed single particle energies calculated in one j-shell and λ and Δ are the Fermi energy and the gap parameter, respectively.

The total wave functions are expanded into the usual strong coupling wave functions with a good projection K of the total angular momentum I to the intrinsic axis "3", which satisfy the symmetry condition under rotation $R_2(\pi)$ around the "2" axis [6]),

$$|IM\rangle = \sum_{K>0,\, i} C^I_{Ki} |IMKi\rangle, \tag{5}$$

where

$$\begin{aligned} |IMKi\rangle &= N_I \{ D^I_{MK} \alpha^+_i |\text{BCS}\rangle + (-)^{I-K+l} D^I_{M-K} \alpha^+_{\bar{i}} |\text{BCS}\rangle \}, \\ &\qquad \text{for mod } (K - \tfrac{1}{2}, 2) = 0, \\ |IMKi\rangle &= N_I \{ D^I_{MK} \alpha^+_i |\text{BCS}\rangle + (-)^{I-K+l+1} D^I_{M-K} \alpha^+_{\bar{i}} |\text{BCS}\rangle \}, \\ &\qquad \text{for mod } (K - \tfrac{1}{2}, 2) = 1, \end{aligned} \tag{6}$$

in which the normalization factor $N_I = \sqrt{(2I+1)/16\pi^2}$.

To be able to introduce the variable moment of inertia (VMI) for the core, the basis states (6) are expanded in terms of eigenfunctions of the angular momentum squared $\hat{R}^2$ of the core:

$$|IMR\alpha j\rangle = \sum_{M_R m} (RM_R jm|IM)|R\alpha M_R\rangle \beta^+_{jm}|\mathrm{BCS}\rangle. \tag{7}$$

Here $|R\alpha M_R\rangle$ are the wave functions of the core [7]) and β^+_{jm} are the creation operator of spherical quasi-particles in the lab system. They are defined in the spherical basis and connected with the α^+_i in the following way:

$$\beta^+_{jm} = \sum_{\Omega} D^j_{m\Omega}\beta^+_{j\Omega} = \sum_{\Omega} D^j_{m\Omega} \sum_i W^i_\Omega \alpha^+_i. \tag{7a}$$

Thus

$$\sum_{n=1}^{3} \frac{R_n^2}{2\theta_{nR}} |R\alpha M_R\rangle = E_{R\alpha}|R\alpha M_R\rangle, \tag{8}$$

and $|R\alpha M_R\rangle$ can be expressed as

$$|R\alpha M_R\rangle = \sum_{N \geq 0} A^\alpha_N N_R \{D^R_{m_R N} + (-)^R D^R_{M_R - N}\}, \tag{9}$$

where N should be even and $N_R = \sqrt{(2R+1)/16\pi^2(1+\delta_{N,0})}$. The mixing coefficients A^α_N are determined by diagonalizing the usual Hamiltonian matrix

$$\sum_{N'} \langle RNM_R| \sum_{n=1}^{3} \frac{R^2}{2\theta_{nR}} |RN'M_R\rangle A^\alpha_{N'} = E_{R\alpha} A^\alpha_N, \tag{9a}$$

with

$$|RNM_R\rangle = N_R\{D^R_{M_R N} + (-)^R D^R_{M_R - N}\},$$

of the asymmetric rotator of Davydov and Filippov [7]) for an even-mass nucleus. Appropriately symmetrized basis functions (7) have the form:

$$|IMR\alpha j\rangle = \sum_{N \geq 0, q} A^\alpha_N N_R \{(RNjq|IN+q)D^I_{MN+q} + (-)^R (R-Njq|I\ -N+q)D^I_{M\ -N+q}\}\beta^+_{jq}|\mathrm{BCS}\rangle. \tag{10}$$

The matrix elements of the total Hamiltonian are written as

$$\langle IMKi|H|IMK'i'\rangle = E_i \delta_{K,K'}\delta_{i,i'} + \sum_{R\alpha} \langle IMKi|IMR\alpha j\rangle E_{R\alpha} \langle IMR\alpha j|IMK'i'\rangle, \tag{11}$$

where $\langle IMKi|IMR\alpha j\rangle$ are the overlap matrix elements, which are written as

$$\langle IMKi|IMR\alpha j\rangle = \frac{1}{2}\sqrt{\frac{2R+1}{2I+1}}\left\{\sum_q^u \frac{A^\alpha_{K-q}}{\sqrt{1+\delta_{K-q,0}}}(R\,K-q\;jq|IK)W^i_q + \sum_q^u (-)^R \right.$$

$$\times \frac{A^\alpha_{q-K}}{\sqrt{1+\delta_{K-q,0}}}(R\,K-q\;jq|IK)W^i_q + \sum_q^d \frac{A^\alpha_{-K-q}}{\sqrt{1+\delta_{-K-q,0}}}(R-K-q\;jq|I-K)$$

$$\left.\times W^i_{-q}(-)^{I-j} + \sum_q^d \frac{A^\alpha_{K+q}}{\sqrt{1+\delta_{-K-q,0}}}(R\;-K-q\;jq|I-K)W^i_{-q}(-)^{R+I-j}\right\}, \qquad (12a)$$

for mod $(K-\frac{1}{2}, 2) = 0$,

$$\langle IMKi|IMR\alpha j\rangle = \frac{1}{2}\sqrt{\frac{2R+1}{2I+1}}\left\{\sum_q^d \frac{A^\alpha_{K-q}}{\sqrt{1+\delta_{K-q,0}}}(R\,K-q\;jq|IK)W^i_{-q}(-)^{I-J}\right.$$

$$+ \sum_q^d \frac{A^\alpha_{q-K}}{\sqrt{1+\delta_{K-q,0}}}(R\,K-q\;jq|IK)W^i_{-q}(-)^{R+I-j} + \sum_q^u \frac{A^\alpha_{-K-q}}{\sqrt{1+\delta_{-K-q,0}}}$$

$$\left.\times(R-K-q\;jq|I-K)W^i_q + \sum_q^u \frac{A_{K+q}}{\sqrt{1+\delta_{-K-q,0}}}(R-K-q\;jq|I-K)W^i_q(-)^R\right\}$$

$$\times(-)^{I-K+l+1}, \qquad \text{for mod } (K-\tfrac{1}{2}, 2) = 1. \qquad (12b)$$

Here the symbols u and d on the summation over q indicate the restriction to mod $(q-\frac{1}{2}, 2) = 0$ and mod $(q-\frac{1}{2}, 2) = 1$, respectively. An extension of the VMI model to asymmetric deformed nuclei is chosen in order to take into account the softness of the core [4]). The VMI description for axially symmetric nuclei is based on the equations:

$$E_R(\theta_{0R}) = \frac{\hbar^2}{2\theta_{0R}}R(R+1) + \tfrac{1}{2}C\left[\frac{\theta_{0R}}{\hbar^2} - \frac{\theta_{00}}{\hbar^2}\right]^2, \qquad (13)$$

$$\partial E_R/\partial\theta_{0R} = 0. \qquad (14)$$

Here θ_{0R} is the moment of inertia for an axially symmetric even-mass nucleus for the angular momentum R. Minimization of the rotational energy E_R as a function of the moment of inertia θ_{0R} according to eq. (14) yields the VMI equation for axially symmetric nuclei.

$$\varepsilon_R^3 - \varepsilon_0\varepsilon_R^2 - \frac{1}{2C}R(R+1) = 0, \qquad (15)$$

where $\varepsilon_R = \theta_{0R}/\hbar^2$ and $\varepsilon_0 = \theta_{00}/\hbar^2$. The moment of inertia θ_{0R} which depends on the angular momentum is given by solving the VMI equation (15). We now extend the VMI model to an asymmetric nucleus by assuming that for a nucleus with three different moments of inertia ($n = 1, 2, 3$)

$$\theta_{nR} = \tfrac{4}{3}\theta_{0R}\sin^2(\gamma - \tfrac{2}{3}\pi n),$$

and that relation (15) determines the common factor θ_{0R} in front of all three moments. The extension of the VMI model to an asymmetric ($\gamma \neq 0$) rotator can only be done by an additional assumption. The method given above seems to be reasonable and simple, since it reduces to the usual VMI model for $\gamma = 0$. The only additional assumption is that the third moment of inertia θ_{3R} for the rotation around the intrinsic z-axis varies with increasing angular momentum R in the same way as the angular momenta θ_{1R} and θ_{2R} for the rotation around the intrinsic x- and y-axes. The two parameters θ_{00} and C which fix the variation of θ_{0R} and therefore also of θ_{1R}, θ_{2R} and θ_{3R} in the extended VMI model are determined by the first 2^+ and first 4^+ energies. In this way our description combines the asymmetric rotor [7]) and the VMI model [4]). (Another recipe for the extension of the VMI model to an asymmetric deformed even-mass nucleus would be the minimization of the energy eigenvalues $E_{R\,\text{ground}}$ of the asymmetric rotator (8) plus the potential energy $\frac{1}{2}C(\theta_{0R}-\theta_{00})^2/\hbar^4$ as a function of θ_{0R}. By fitting the energies for the first 2^+ and the 4^+ states one could determine the moment of inertia parameter θ_{00} and the stiffness parameter C. But the results are not changed appreciably with respect to the simpler procedure outlined above.)

3. Moments and transitions

The E2 and M1 operators are given in lab system [8]) by:

$$\mathcal{M}(\mathrm{E2};\mu) = \left(\delta_\mathrm{p} + \frac{Z}{A^2}\right) r^2 Y_{2\mu}(\theta,\zeta) + \frac{3}{4\pi} Z R_0^2 \alpha^*_{2\mu}, \tag{16}$$

$$\begin{aligned}\mathcal{M}(\mathrm{M1};\mu) &= \mu_\mathrm{n}\left(\frac{3}{4\pi}\right)^{\frac{1}{2}} \{g_R I_\mu + (g_l - g_R) j_\mu + (g_s - g_l) s_\mu\} \\ &= \mu_\mathrm{n}\left(\frac{3}{4\pi}\right)^{\frac{1}{2}} \{g_R I_\mu + G_\mu\},\end{aligned} \tag{17}$$

where the various symbols ocurring in eqs. (16) and (17) have their usual meaning. Here Z and A are the charge and mass number, respectively; $R_0 = 1.2\, A^{\frac{1}{3}}$ fm is the nuclear radius and $\alpha_{2\mu}$ describes the quadrupole deformation of the nucleus. The effective charge δ_p has the value 1.5 for protons and 0.5 for neutrons in our calculations. In addition I_μ, j_μ and s_μ are the total, single particle and spin angular momentum, respectively. Here $\mu_\mathrm{n} = e\hbar/2mc$ denotes the nuclear magneton and the values used for the g-factors are

$$g_s = \begin{cases} 5.59 & \text{for protons} \\ -3.83 & \text{for neutrons,} \end{cases} \tag{18}$$

$$g_l = \begin{cases} 1 & \text{for protons} \\ 0 & \text{for neutrons,} \end{cases} \tag{19}$$

$$g_R = Z/A. \tag{20}$$

The B(E2) and B(M1) values are defined as

$$B(\lambda; I_i \to I_f) = \frac{2I_f+1}{2I_i+1} \sum_{M_i M_f \mu} |\langle I_i M_i | \mathcal{M}(\lambda\mu) | I_f M_f \rangle|^2 = \frac{2I_f+1}{2I_i+1} |\langle I_i || \mathcal{M}(\lambda) || I_f \rangle|^2, \quad (21)$$

where we use the Wigner-Eckert theorem in the form:

$$\langle I_i M_i | \mathcal{M}(\lambda\mu) | I_f M_f \rangle = [(2I_f+1)/(2I_i+1)]^{\frac{1}{2}} (I_f M_f \lambda\mu | I_i M_i) \langle I_i || \mathcal{M}(\lambda) || I_f \rangle. \quad (22)$$

We calculate the mixing ratios δ for the E2 and M1 transitions using the relation [9])

$$\delta = 8.78 \times 10^{-4} E_{if} \frac{\langle I_i || \mathcal{M}(\mathrm{E2}) || I_f \rangle}{\langle I_i || \mathcal{M}(\mathrm{M1}) || I_f \rangle}, \quad (23)$$

where $E_{if} = E_i - E_f$ is the transition energy in MeV and the reduced matrix elements $\langle I_i || \mathcal{M}(\mathrm{E2}) || I_f \rangle$ and $\langle I_i || \mathcal{M}(\mathrm{M1}) || I_f \rangle$ are calculated in $e \cdot \mathrm{fm}^2$ and $e \cdot \mathrm{fm}$, respectively. It is evident from eq. (23) that the ratio of the E2 transition to that of the M1 transition is equal to δ^2. From the reduced matrix elements $\langle I_i || \mathcal{M}(\lambda) || I_f \rangle$ in eq. (22), one obtains the expressions for the quadrupole and the magnetic moments in the lab system as

$$Q_I = (II20|II)\sqrt{\tfrac{16}{5}\pi} \langle I || \mathcal{M}(\mathrm{E2}) || I \rangle, \quad (24)$$

$$\mu_I = (II20|II)\sqrt{\tfrac{4}{3}\pi} \langle I || \mathcal{M}(\mathrm{M1}) || I \rangle. \quad (25)$$

In order to calculate the reduced matrix elements in eqs. (21)–(25), the operators $\mathcal{M}(\lambda\mu)$ must be expressed in the body-fixed system using D-functions.

$$\mathcal{M}(\lambda\mu) = \sum_\nu D^\lambda_{\mu\nu} \mathcal{M}(\lambda\nu), \quad (26)$$

from which one obtains the expressions for the E2 and M1 operators given by

$$\mathcal{M}(\mathrm{E2}; \mu) = \left(\delta_p + \frac{Z}{A^2}\right) \sum_\nu D^2_{\mu\nu} r^2 Y_{2\nu}(\vartheta, \zeta) + \frac{3}{4\pi} Z R_0^2 \left[D^2_{\mu 0} \beta \cos\gamma + (D^2_{\mu 2} + D^2_{\mu -2}) \frac{\beta}{\sqrt{2}} \sin\gamma \right], \quad (27)$$

$$\mathcal{M}(\mathrm{M1}; \mu) = \mu_n \left(\frac{3}{4\pi}\right)^{\frac{1}{2}} \sum_\nu D^1_{\mu\nu} \{ g_R I_\nu + G_\nu \}, \quad (28)$$

with

$$G_\nu = (g_l - g_R) j_\nu + (g_s - g_l) s_\nu.$$

Then using relations (27) and (28), a straightforward calculation gives the desired matrix elements for the E2 and M1 transitions as

$$\langle I_i||\mathscr{M}(E2)||I_f\rangle = \left(\delta_p + \frac{Z}{A^2}\right)\{\sum_{\substack{Ki,K'i'}}^{\substack{u,u'\\d,d'}} C^{I_i}_{Ki}\, C^{I}_{K'i'} \sum_{\nu} [(I_f K'2 \pm \nu|I_i K)\langle i|r^2 Y_{2\nu}|i'\rangle$$

$$\times (u_i u_{i'} - v_i v_{i'}) + \delta_{i,i'}(I_f k'2\nu|I_i K) \sum_{j>0} 2v_j^2 \langle j|r^2 Y_{2\nu}|j\rangle + (I_f k'2 \mp \nu|I_i - K)$$

$$\times (-)^{I_i - \frac{1}{2} + l}\langle i|r^2 Y_{2\nu}|\bar{\imath}\rangle (u_i u_{i'} - v_i v_{i'})] + \sum_{\substack{Ki,K'i'}}^{\substack{u,d'\\d,u'}} C^{I_i}_{Ki} C^{I_f}_{K'i'} \sum_{\nu} [(I_f K'2 \pm \nu|I_i K)$$

$$\times \langle i|r^2 Y_{2\nu}|\bar{\imath}\rangle (u_i u_{i'} - v_i v_{i'}) + (-)^{I_i - \frac{1}{2} + l}(I_f K'2\nu|I_i - K)\delta_{i,i'} \sum_{j>0} 2v_j^2 \langle j|r^2 Y_{2\nu}|j\rangle\}$$

$$+ \frac{3}{4\pi} ZR_0^2 \beta \{\sum_{\substack{Ki,K'i'}}^{\substack{u,u'\\d,d'}} \delta_{i,i'} C^{I_i}_{Ki} C^{I_f}_{K'i'}[(I_f K'20|I_i K)\cos\gamma$$

$$+ ((I_f K'22|I_i K) + (I_f K'2 - 2|I_i K))\sqrt{\tfrac{1}{2}}\sin\gamma]$$

$$+ \sum_{\substack{Ki,K'i'}}^{\substack{u,d'\\d,u'}} \delta_{i,i'} C^{I_i}_{Ki} C^{I_f}_{K'i'} (-)^{I_i - \frac{1}{2} + l}(I_f K'2 - 2|I_i - K)\sqrt{\tfrac{1}{2}}\sin\gamma\}, \tag{29}$$

$$\langle I_i||\mathscr{M}(M1)||I_f\rangle = \mu_n \left(\frac{3}{4\pi}\right)^{\frac{1}{2}} \{\sum_{\substack{Ki,K'i'}}^{\substack{u,u'\\d,d'}} C^{I_i}_{KI} C^{I_f}_{K'i'}(u_i u_{i'} + v_i v_{i'})$$

$$\times \sum_{\nu} (\pm 1)[(I_f K'1\nu|I_i K)\langle i|G_\nu|i'\rangle - (I_f K'1 \mp \nu|I_i - K)(-)^{I_i - \frac{1}{2} + l}\langle i|G_\nu|\bar{\imath}\rangle]$$

$$+ \sum_{\substack{Ki,K'i'}}^{\substack{u,d'\\d,u'}} C^{I_i}_{Ki} C^{I_f}_{K'i'}(u_i u_{i'} + v_i v_{i'}) \sum_{\nu} (\pm 1)(I_f K'1 \pm \nu|I_i K)\langle i|G_\nu|\bar{\imath}\rangle$$

$$+ g_R \sum_{\substack{Ki,K'i'}}^{\substack{u,u'\\d,d'}} \delta_{i,i'}\delta_{K,K'} C^{I_i}_{Ki} C^{I_f}_{K'i'}\{(-\sqrt{\tfrac{1}{2}})[(I_f + K')(I_f - K' + 1)]^{\frac{1}{2}}(I_f K' - 111|I_i K)$$

$$+ \sqrt{\tfrac{1}{2}}[(I_f - K')(I_f + K' + 1)]^{\frac{1}{2}}(I_f K' + 11 - 1|I_i K) + K'(I_f K'10|I_i K)\}, \tag{30}$$

in which the symbols u and d (u' and d') restrict the summation over $K(K')$ to $\mathrm{mod}\,(K - \frac{1}{2}, 2) = 0$ and $\mathrm{mod}\,(K - \frac{1}{2}, 2) = 1$ ($\mathrm{mod}\,(K' - \frac{1}{2}, 2) = 0$ and $\mathrm{mod}\,(K' - \frac{1}{2}, 2) = 1$), respectively. In eqs. (29) and (30) the upper signs correspond to the upper combinations (u, u') or (u, d') whereas the lower signs are to be used for the lower combinations (d, d') or (d, u'). Furthermore, the single particle reduced matrix elements occurring in these equations are given by

$$\langle i|O_{\lambda\nu}|i'\rangle = \langle j||O_\lambda||j\rangle \sum_{mm'} W^i_m(jm'\lambda\nu|jm) W^{i'}_{m'}, \tag{31}$$

$$\langle i|O_{\lambda\nu}|i'\rangle = \langle j||O_\lambda||j\rangle \sum_{mm'} W_m^i (j-m'\lambda\nu|jm)(-)^{l+j-m'} W_{m'}^{i'}, \tag{32}$$

where $\langle j||O_\lambda||j\rangle$ corresponding to operators $r^2 Y_2$ and G for O_λ are

$$\langle j_l||r^2 Y_2||j\rangle = \frac{\hbar}{m\omega}\sqrt{\frac{2j+1}{4\pi}}(-)^{j-\frac{1}{2}}(j\tfrac{1}{2}\ j-\tfrac{1}{2}|20)(N+\tfrac{3}{2}) \tag{33}$$

$$\langle j||G||j\rangle = (g_l-g_R)[j(j+1)]^{\frac{1}{2}} + (g_s-g_l)\tfrac{1}{2}[\tfrac{3}{4}+j(j+1)-l(l+1)]/[j(j+1)]^{\frac{1}{2}}, \tag{34}$$

in which N is the principal quantum number of the single particle state and $\hbar/m\omega = 1.01\ A^{\frac{1}{3}}$ fm^2.

4. Results

Calculations in the above developed model are performed for Ir, Au and Hg isotopes near the $A \approx 190$ region, and for ^{135}Pr and ^{133}La. The excitation energies of adjacent even-mass nuclei which are used in the calculation of the odd-mass nuclei are listed in table 1. These excitation energies are well reproduced combining the VMI [4]) and the asymmetric rotator model [7]) as discussed in sect. 2. For the calculation of the odd-mass nuclei we take the averaged values of the empirical

TABLE 1

Experimental excitation energies (keV) in even-mass nuclei which are used in the calculation of odd-mass nuclei

I^π	$^{186}_{76}Os_{110}$	$^{188}_{76}Os_{112}$	$^{188}_{78}Pt_{110}$	$^{190}_{78}Pt_{112}$	$^{192}_{78}Pt_{114}$	$^{194}_{78}Pt_{116}$
2^+	137.2	155.0	265.9	295.7	316.5	328.5
4^+	433.9	477.9	671.3	736.9	784.6	811.1
6^+	868.7	938.8	1184.6	1287.5	1365.3	1411.6
8^+	1420.5	1513.6	1782.0	1915.1	2018.1	2099.4
10^+	2068.1	2169.5	2436.0	2535.1	2518.7	

I^π	$^{190}_{80}Hg_{110}$	$^{192}_{80}Hg_{112}$	$^{194}_{80}Hg_{114}$	$^{196}_{80}Hg_{116}$	$^{132}_{56}Ba_{76}$	$^{134}_{58}Ce_{76}$	$^{136}_{60}Nd_{76}$
2^+	416.2	422.8	427.9	426.1	465.0	409.0	374.0
4^+	1041.6	1057.6	1064.3	1061.4	1128.0	1049.0	974.0
6^+	1772.6	1803.0	1799.0	1784.9	1938.0	1863.0	1720.0
8^+	2464.4	2446.8	2363.7	2262.6		2811.0	2530.0
10^+	2596.2	2506.9	2433.3	2359.6			
12^+	3015.8	2923.2	2836.2	2764.4			
14^+		3579.9	3479.0				
16^+		4360.7	4222.8				
18^+		5102.1	4933.1				

For other energies of the even-mass core the theoretical values of the asymmetric rotor generalized by the inclusion of the VMI model are used [see eqs. (8) and (15)]. This ensures that the results depend only slightly on θ_{00} and C.

excitation energies (as far as known) of the adjacent even nuclei. Throughout the calculation we have used the gap energy $\Delta = 12/\sqrt{A}$ MeV [ref. [10])], which gives the general trend in the observed gap energy. The constant of the gap energy is not sensitive to the results. Further, we took the empirical relation between θ_{02} and β [see definitions after eq. (15)]:

$$\theta_{02} = 3B\beta^2 = \tfrac{3}{1225}A^{\frac{7}{3}}\beta^2 \tag{35}$$

to determine the β-deformation. The relation is derived from the empirical relation between the excitation energy of the first 2^+ state and the B(E2) value of the transition from the first 2^+ state to the ground state of almost all nuclei given by Grodzins [11]).

We calculated the excitation energies without using the relation (35), but the results were not improved.

The minimization of the χ^2 proceeds in the following way:

(i) For the parameters γ and λ an initial value is assumed.

(ii) The eigenvalue problem (8) for even-mass nuclei with the γ as given above is solved for the 2_1^+ and 4_1^+ states. This yields the moments of inertia $\varepsilon_2 = \hbar^2/\theta_{02}$ and $\varepsilon_4 = \hbar^2/\theta_{04}$. Solution of eq. (15) gives the parameters θ_{00} and C of the VMI model.

(iii) The total Hamiltonian for the odd-mass nucleus is solved and the χ^2 value using data of the odd-mass nucleus is calculated according to

$$\chi^2 = \frac{1}{N-2}\sum_{n=1}^{N}\frac{(E_n(\text{exp})-E_n(\text{th}))^2}{\Delta E_n}, \tag{36}$$

where N is the number of data, E_n(exp) and E_n(th) are the experimental and the theoretical values, and ΔE_n is the experimental error.

(iv) The minimization procedure Simplex [5]) yields an improved set of parameters λ and γ and one goes back to point (ii) until the method converges.

4.1. ISOTOPES IN THE Au REGION

In figs. 1, 2 and 3 the measured decoupled bands built on single particle states of Hg, Au and Ir isotopes [1]) are compared with our model calculations. The results of Meyer-ter-Vehn [3, 12]) for the nuclei ^{193}Hg, ^{195}Au and ^{187}Ir are also shown for the purpose of comparison. In our calculations the parameters (γ and λ) used are those obtained by minimization procedure and the values of the parameters for various isotopes studied are given along with the figs. 1, 2 and 3. It may be noted that the values of the parameters β and γ used by Meyer-ter-Vehn are near to those obtained by us in minimization procedures. It means that the procedure taken by Meyer-ter-Vehn to use the experimental excitation energies of the adjacent even-mass nuclei in order to get β- and γ-deformations works very nicely and one can learn many things about the properties of the core by studying the low-lying high-spin states of odd-mass nuclei.

We see from figs. 1, 2 and 3 that our results for the excitation energies for different

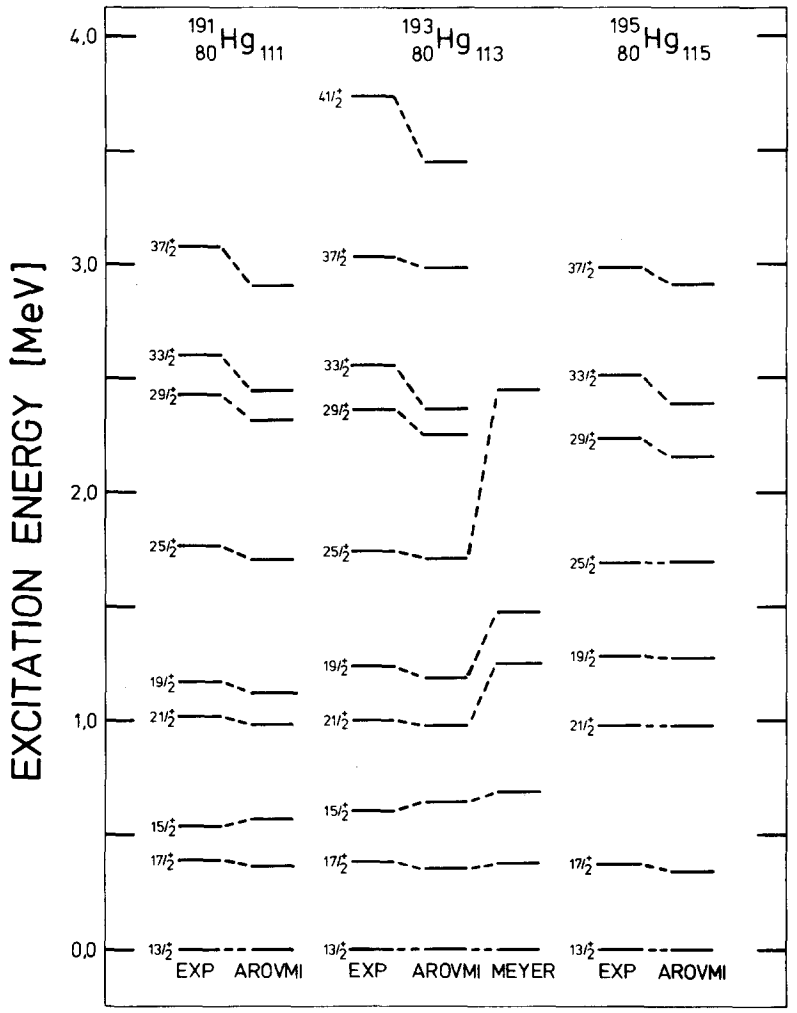

Fig. 1. Experimental and calculated excitation energies of decoupled bands built on an $i_{13/2}$ neutrons of Hg isotopes. The experimental excitation energies for each nuclei are shown on the left. AROVMI denotes the results of our calculations assuming an odd particle coupled to an asymmetric rotor with a variable moment of inertia (asymmetric rotor odd particle VMI). For ^{193}Hg the results of Meyer-ter-Vehn [3, 10] are also shown. Parameters used in our calculations are (i) $\beta = 0.137$, $\gamma = 37.2°$, $\lambda = 0.686$ MeV, $\theta_{00}/\hbar^2 = 8.35$ MeV^{-1}, $C = 0.0246$ MeV^3 for ^{191}Hg, (ii) $\beta = 0.128$, $\gamma = 41.7°$, $\lambda = 0.986$ MeV, $\theta_{00}/\hbar^2 = 6.33$ MeV^{-1}, $C = 0.0176$ MeV^3 for ^{193}Hg, (iii) $\beta = 0.124$, $\gamma = 43.2°$, $\lambda = 1.87$ MeV, $\theta_{00}/\hbar^2 = 5.77$ MeV^{-1}, $C = 0.0170$ MeV^3 for ^{195}Hg. For the ground-state rotational energies of the core E_R the mean value of the neighbouting even-mass nuclei tabulated in table 1 has been used. The low-lying spin states with $I < j$ are tabulated in table 2.

isotopes are in nice agreement with experiments. A comparison of our results with those of Meyer-ter-Vehn who has used the rigid asymmetric rotor model reveals the importance of the inclusion of the softness of the core. The excitation energies of

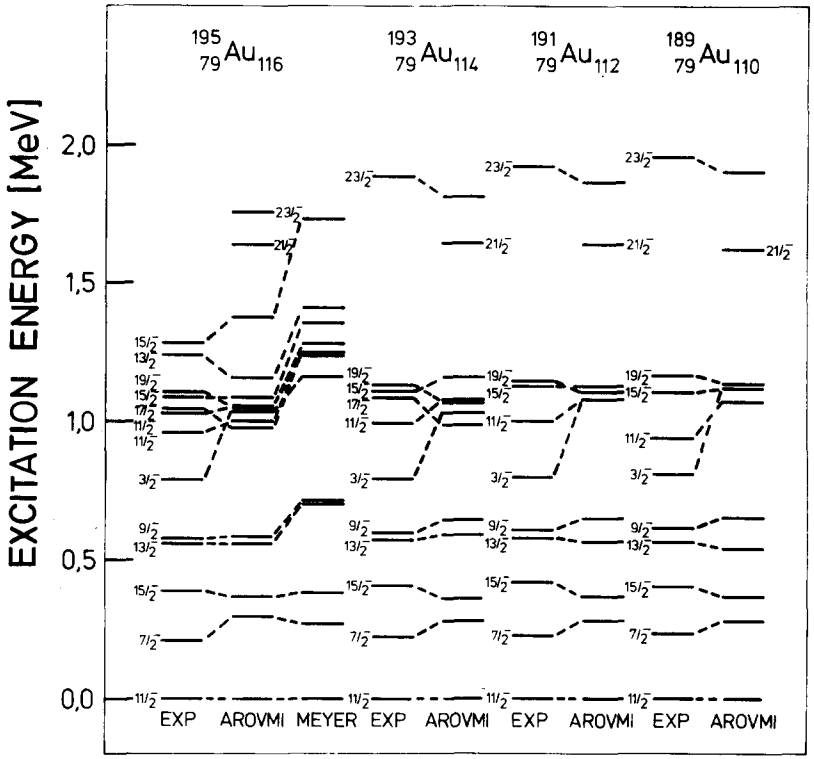

Fig. 2. Experimental and calculated excitation energies of decoupled bands built on a $h_{\frac{11}{2}}$ proton of Au isotopes. Abbreviations used are explained in fig. 1. Parameters used in our calculations are (i) $\beta = 0.144$, $\gamma = 35.5°$, $\lambda = 1.61$ MeV, $\theta_{00}/\hbar^2 = 9.99$ MeV^{-1}, $C = 0.0211$ MeV^3 for ^{195}Au, (ii) $\beta = 0.146$, $\gamma = 35.5°$, $\lambda = 2.12$ MeV, $\theta_{00}/\hbar^2 = 9.90$ MeV^{-1}, $C = 0.0189$ MeV^3 for ^{193}Au, (iii) $\beta = 0.152$, $\gamma = 34.8°$, $\lambda = 2.40$ MeV, $\theta_{00}/\hbar^2 = 10.81$ MeV^{-1}, $C = 0.0212$ MeV^3 for ^{191}Au, (iv) $\beta = 0.159$, $\gamma = 34.1°$, $\lambda = 3.55$ MeV, $\theta_{00}/\hbar^2 = 11.89$ MeV^{-1}, $C = 0.0234$ MeV^3 for ^{189}Au. The ground state rotational energies of the core are taken from experiment (see fig. 1 caption).

especially the higher-spin states ($I > j$) obtained with the rigid asymmetric rotor model are always higher compared to experimental ones.

As can be seen from fig. 1, the experimental spectra of Hg isotopes have an anomaly around $I = \frac{29}{2}^+$ and $\frac{33}{2}^+$ states where the spacing of the favoured band does not increase monotonically but decreases abruptly. (This corresponds to the anomaly near $I = 8^+$ and 10^+ states in the ground rotational band of the even-mass Hg nuclei.) This anomaly is reproduced by our treatment when we use the experimental values as far as known for the core excitation energies instead of the VMI predicted values. The excitation energies of the favoured bands are very sensitive to the core excitation energies and are very similar to the ground-state rotational spectrum of the even-mass nuclei. It is interesting to note that this feature is also manifested in the experimental values. The reason why the odd and the even Hg isotopes have very similar rotational

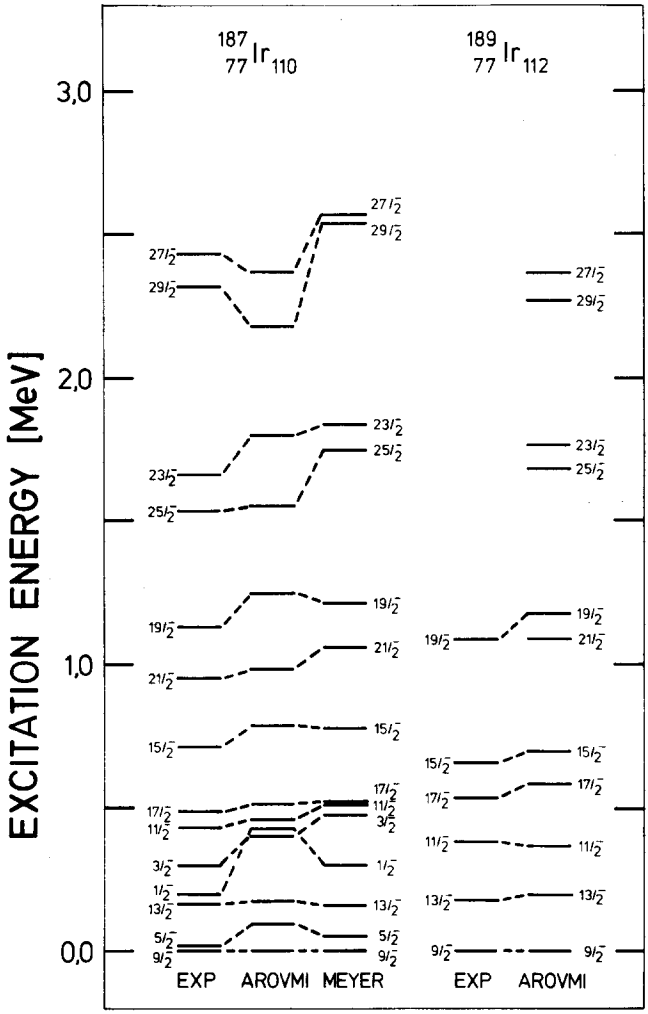

Fig. 3. Experimental and calculated excitation energies of decoupled bands built on a $h_{\frac{9}{2}}$ proton of Ir isotopes. Abbreviations used are explained in fig. 1. Parameters used in our calculations are (i) $\beta = 0.178$, $\gamma = 8.4°$, $\lambda = -1.29$ MeV, $\theta_{00}/\hbar^2 = 12.86$ MeV^{-1}, $C = 0.00477$ MeV^3 for ^{187}Ir, (ii) $\beta = 0.190$, $\gamma = 23.2°$, $\lambda = -1.15$ MeV, $\theta_{00}/\hbar^2 = 17.07$ MeV^{-1}, $C = 0.00935$ MeV^3 for ^{189}Ir. The ground-state rotational energies of the core are taken from experiment in even-mass nuclei (see fig. 1 caption).

spectrum is the following. The deformation parameters β of these nuclei are small ($\beta \approx 0.13$) which gives rise to a large Coriolis force. And this large Coriolis force favours the decoupling, and the total wave function of the favoured band of the odd nucleus consists mainly of the odd particle coupled to the core with angular momentum $R = I - j$ as may be seen by the overlap matrix

$$\langle IMR\alpha j|IM\rangle = \sum_{Ki} C^{I}_{Ki}\langle IMR\alpha j|IMKi\rangle, \tag{37}$$

which have values $\langle IMR = I-j\alpha = 1j|IM\rangle \approx 0.97$.

In the case of Au isotopes (see fig. 2) it is seen that though the higher-spin states ($I > j$) come down to the corresponding experimental excitation energies from the rigid rotor predicted values by introducing the softness of the core, the lower-spin states $\frac{7}{2}^-$ and $\frac{3}{2}^-$ are still high compared with the experimental energies. These lower-spin states are not so sensitive to the change of the parameters γ and λ. (Variation of γ and λ by 10% from the values obtained by minimization procedure does not affect the trend.) However, this discrepancy at lower-spin states is found to be a common feature for the isotopes considered with our model. This may be remedied by considering additional single particle levels not included in our model.

Our results for the excitation energies, quadrupole and magnetic moments, B(E2) and B(M1) values, and also the mixing ratios for E2 and M1 transitions for the Hg, Au and Ir isotopes are displayed in tables 2 and 3, 4 and 5, and 6 and 7, respectively. From tables 3, 5 and 7 of the calculated $B(\mathrm{E2}, I_i \to I_f)$ and $B(\mathrm{M1}, I_i \to I_f)$

TABLE 2

Calculated excitation energies (keV) relative to the $I^\pi = \frac{13}{2}^+$ state, spectroscopic quadrupole moments ($e\cdot$b) and magnetic moments ($e\cdot$fm) of yrast states in Hg isotopes

I	^{191}Hg			^{193}Hg			^{195}Hg		
	E	Q	μ	E	Q	μ	E	Q	μ
$\frac{41}{2}$	4836	0.61	0.42	3449	0.91	0.42	4966	1.10	0.41
$\frac{39}{2}$	4957	0.62	0.44	3585	0.90	0.44	5043	1.11	0.43
$\frac{37}{2}$	2904	0.61	0.33	2794	0.94	0.33	2912	1.10	0.32
$\frac{35}{2}$	3068	0.60	0.34	2928	0.92	0.35	3095	1.06	0.33
$\frac{33}{2}$	2444	0.65	0.25	2364	0.97	0.25	2384	1.17	0.25
$\frac{31}{2}$	2558	0.69	0.27	2480	0.98	0.27	2466	1.14	0.26
$\frac{29}{2}$	2310	0.72	0.18	2252	1.05	0.18	2155	1.28	0.19
$\frac{27}{2}$	2390	0.81	0.19	2310	1.09	0.20	2173	1.24	0.21
$\frac{25}{2}$	1705	0.76	0.07	1711	1.16	0.07	1701	1.46	0.08
$\frac{23}{2}$	1823	1.00	0.07	1859	1.18	0.07	1822	1.35	0.10
$\frac{21}{2}$	983	0.94	−0.02	977	1.32	−0.02	979	1.58	−0.02
$\frac{19}{2}$	1116	1.11	−0.03	1185	1.17	−0.02	1275	1.30	−0.01
$\frac{17}{2}$	360	1.27	−0.10	352	1.36	−0.11	346	1.55	−0.10
$\frac{15}{2}$	572	0.92	−0.12	646	0.92	−0.11	797	1.08	−0.11
$\frac{13}{2}$	0	1.11	−0.19	0	1.14	−0.19	0	1.40	−0.19
$\frac{11}{2}$	449	0.57	−0.19	527	0.44	−0.19	688	0.67	−0.18
$\frac{9}{2}$	311	0.67	−0.26	293	0.82	−0.26	266	1.14	−0.25
$\frac{7}{2}$	910	0.38	−0.22	950	0.03	−0.21	1052	0.22	−0.20
$\frac{5}{2}$	940	0.35	−0.29	913	0.44	−0.29	867	0.70	−0.29
$\frac{3}{2}$	1656	0.00	−0.10	1657	−0.22	−0.09	1683	−0.29	−0.09
$\frac{1}{2}$	1644		−0.17	1653		−0.16	1633		−0.16

The $I^\pi = \frac{13}{2}^+$ state constitutes the band head of the favoured decoupled band built on the $i_{\frac{13}{2}}$ neutron level at x (not known), 141 and 176 keV, respectively [eqs. (21), (29)].

TABLE 3

Calculated B(E2) ($e^2 \cdot b^2$) and B(M1) ($e^2 \cdot fm^2 \times 10^{-2}$) values and mixing ratios [eq. (23)] of the transitions between yrast states in Hg isotopes

I_i	I_f	^{191}Hg			^{193}Hg			^{195}Hg		
		B(E2)	B(M1)	δ	B(E2)	B(M1)	δ	B(E2)	B(M1)	δ
$\frac{41}{2}$	$\frac{39}{2}$	0.00	0.65	−0.01	0.00	0.65	0.00	0.00	0.66	−0.01
$\frac{41}{2}$	$\frac{37}{2}$	0.78			0.66			0.54		
$\frac{39}{2}$	$\frac{37}{2}$	0.03	0.01	−3.09	0.03	0.06	−0.48	0.03	0.03	−1.88
$\frac{39}{2}$	$\frac{35}{2}$	0.73			0.63			0.50		
$\frac{37}{2}$	$\frac{35}{2}$	0.00	0.60	0.0	0.00	0.63	0.0	0.00	0.57	0.0
$\frac{37}{2}$	$\frac{33}{2}$	0.74			0.64			0.51		
$\frac{35}{2}$	$\frac{33}{2}$	0.04	0.09	−0.37	0.03	0.09	−0.30	0.03	0.18	−0.25
$\frac{35}{2}$	$\frac{31}{2}$	0.67			0.60			0.47		
$\frac{33}{2}$	$\frac{31}{2}$	0.00	0.64	−0.01	0.00	0.63	0.0	0.00	0.67	0.0
$\frac{33}{2}$	$\frac{29}{2}$	0.71			0.59			0.47		
$\frac{31}{2}$	$\frac{29}{2}$	0.05	0.21	−0.11	0.04	0.26	−0.08	0.03	0.49	−0.07
$\frac{31}{2}$	$\frac{27}{2}$	0.65			0.54			0.45		
$\frac{29}{2}$	$\frac{27}{2}$	0.01	0.70	−0.01	0.00	0.73	0.0	0.01	0.90	0.0
$\frac{29}{2}$	$\frac{25}{2}$	0.65			0.52			0.45		
$\frac{27}{2}$	$\frac{25}{2}$	0.07	0.02	−1.06	0.05	0.03	−0.67	0.05	0.23	−0.18
$\frac{27}{2}$	$\frac{23}{2}$	0.50			0.45			0.44		
$\frac{25}{2}$	$\frac{23}{2}$	0.01	0.44	−0.02	0.00	0.46	0.01	0.00	0.61	0.0
$\frac{25}{2}$	$\frac{21}{2}$	0.63			0.51			0.42		
$\frac{23}{2}$	$\frac{21}{2}$	0.11	0.03	−1.37	0.09	0.03	−1.26	0.07	0.10	−0.61
$\frac{23}{2}$	$\frac{19}{2}$	0.48			0.42			0.37		
$\frac{21}{2}$	$\frac{19}{2}$	0.00	0.34	−0.01	0.02	0.36	0.05	0.01	0.40	0.04
$\frac{21}{2}$	$\frac{17}{2}$	0.51			0.45			0.39		
$\frac{19}{2}$	$\frac{17}{2}$	0.18	0.03	−1.70	0.12	0.04	−1.27	0.10	0.10	−0.80
$\frac{19}{2}$	$\frac{15}{2}$	0.29			0.33			0.32		
$\frac{17}{2}$	$\frac{15}{2}$	0.07	0.23	0.10	0.09	0.25	0.15	0.04	0.30	0.15
$\frac{17}{2}$	$\frac{13}{2}$	0.43			0.40			0.36		
$\frac{15}{2}$	$\frac{13}{2}$	0.25	0.06	−1.08	0.17	0.08	−0.86	0.13	0.15	−0.66

The transition energies E_{if} for the mixing ratios are taken from the theoretical calculation.

values it is seen that the B(E2, $I \to I-2$) values are much larger than the B(E2, $I \to I-1$) values. Also in general the B(M1) values of the transitions from the favoured states ($I-j$ = even) to the unfavoured states ($I-j$ = odd) are larger than those from the unfavoured states to the favoured states. Such regularities are also seen in the mixing ratios δ. The mixing ratios of the transitions from the unfavoured states to the favoured states are much larger than those from the favoured states to the unfavoured states. These regularities are related to the nature of the core and the single particle wave functions of the initial and final states, and to the operator for a particular transition. In this connection we point out that the wave functions of the favoured states ($I = j+2n$; n is an integer) mainly consist of the odd particle coupled to the core with angular momentum $R = I-j = 2n$ (even), whereas those of the unfavoured states ($I = j+2n-1$; n is an integer) mainly consist of the odd particle

TABLE 4

Calculated excitation energies (keV) relative to the $I^\pi = \frac{11}{2}^-$ state, spectroscopic quadrupole moments ($e \cdot$ b) and magnetic moments ($e \cdot$ fm) of yrast states in Au isotopes

I	^{189}Au			^{191}Au			^{193}Au			^{195}Au		
	E	Q	μ	E	Q	μ	E	Q	μ	E	Q	μ
$\frac{25}{2}$	2375	1.26	1.01	2362	1.27	1.01	2333	1.27	1.01	2317	1.08	1.02
$\frac{23}{2}$	1906	1.39	1.00	1863	1.32	1.01	1814	1.31	1.02	1754	1.06	1.03
$\frac{21}{2}$	1620	1.62	0.94	1634	1.55	0.94	1637	1.52	0.94	1638	1.36	0.95
$\frac{19}{2}$	1132	2.16	0.94	1105	1.97	0.95	1071	1.87	0.95	1051	1.52	0.96
$\frac{17}{2}$	937	1.81	0.87	962	1.68	0.87	988	1.62	0.87	978	1.52	0.88
$\frac{15}{2}$	367	2.66	0.87	365	2.47	0.87	360	2.28	0.88	364	2.12	0.88
$\frac{13}{2}$	541	1.52	0.77	563	1.43	0.78	591	1.36	0.78	559	1.27	0.78
$\frac{11}{2}$	0	2.47	0.77	0	2.28	0.78	0	2.12	0.78	0	1.97	0.79
$\frac{9}{2}$	657	0.89	0.63	654	0.86	0.64	647	0.89	0.65	586	0.95	0.66
$\frac{7}{2}$	282	1.90	0.65	284	1.74	0.66	281	1.62	0.66	296	1.40	0.67
$\frac{5}{2}$	1290	0.16	0.42	1205	0.41	0.45	1138	0.41	0.46	1023	0.67	0.48
$\frac{3}{2}$	1118	0.79	0.45	1082	0.70	0.46	1033	0.63	0.47	1042	0.48	0.47
$\frac{1}{2}$	2169		−0.09	2011		−0.10	1905		−0.12	1789		−0.10

The $I^\pi = \frac{11}{2}^-$ state constitutes the band head of the favoured decoupled band built on the $h_{\frac{11}{2}}$ proton level at 247, 266, 290 and 318 keV, respectively.

TABLE 5

Calculated B(E2) ($e^2 \cdot b^2$) and B(M1) ($e^2 \cdot fm^2 \times 10^{-2}$) values and mixing ratios of the transitions between yrast states in Au isotopes (see footnote to table 3).

I_i	I_f	^{189}Au			^{191}Au			^{193}Au			^{195}Au		
		B(E2)	B(M1)	δ	B(E2)	B(M1)	δ	B(E2)	B(M1)	δ	B(E2)	B(M1)	δ
$\frac{25}{2}$	$\frac{23}{2}$	0.18	0.97	0.18	0.14	0.75	0.19	0.12	0.63	0.20	0.11	0.45	0.25
$\frac{25}{2}$	$\frac{21}{2}$	0.64			0.62			0.59			0.63		
$\frac{23}{2}$	$\frac{21}{2}$	0.19	1.12	0.10	0.15	1.02	0.08	0.12	0.97	0.05	0.11	0.92	0.04
$\frac{23}{2}$	$\frac{19}{2}$	0.54			0.54			0.54			0.62		
$\frac{21}{2}$	$\frac{19}{2}$	0.23	0.69	0.25	0.19	0.54	0.28	0.17	0.45	0.30	0.16	0.33	0.35
$\frac{21}{2}$	$\frac{17}{2}$	0.53			0.52			0.50			0.52		
$\frac{19}{2}$	$\frac{17}{2}$	0.10	0.68	0.07	0.08	0.65	0.04	0.06	0.64	0.02	0.07	0.63	0.02
$\frac{19}{2}$	$\frac{15}{2}$	0.41			0.42			0.43			0.46		
$\frac{17}{2}$	$\frac{15}{2}$	0.31	0.47	0.41	0.27	0.40	0.43	0.24	0.35	0.46	0.25	0.26	0.52
$\frac{17}{2}$	$\frac{13}{2}$	0.42			0.40			0.39			0.38		
$\frac{15}{2}$	$\frac{13}{2}$	0.00	0.29	0.01	0.00	0.33	0.00	0.00	0.37	0.00	0.00	0.38	−0.01
$\frac{15}{2}$	$\frac{11}{2}$	0.36			0.36			0.37			0.39		
$\frac{13}{2}$	$\frac{11}{2}$	0.41	0.56	0.41	0.37	0.49	0.43	0.33	0.44	0.45	0.31	0.35	0.49

coupled to the core with angular momentum $R = I - j + 1 = 2n$ (even). On the other hand, the collective part of the E2 operator in eq. (16) which contributes mainly to the B(E2) values has a large matrix element when the cores of the initial and the

TABLE 6

Calculated excitation energies (keV) relative to the $I^\pi = \frac{9}{2}^-$ state, spectroscopic quadrupole moments ($e \cdot$ b) and magnetic moments ($e \cdot$ fm) of yrast states in Ir isotopes

I	^{187}Ir			^{189}Ir		
	E	Q	μ	E	Q	μ
$\frac{29}{2}$	2180	−2.31	0.70	2273	−0.86	0.69
$\frac{27}{2}$	2369	−2.29	0.64	2366	−1.13	0.64
$\frac{25}{2}$	1554	−2.28	0.62	1685	−0.92	0.61
$\frac{23}{2}$	1807	−2.25	0.56	1765	−1.36	0.56
$\frac{21}{2}$	983	−2.25	0.53	1090	−1.01	0.53
$\frac{19}{2}$	1250	−2.22	0.47	1183	−1.49	0.48
$\frac{17}{2}$	515	−2.16	0.44	589	−1.27	0.44
$\frac{15}{2}$	788	−1.93	0.38	701	−1.46	0.39
$\frac{13}{2}$	174	−1.97	0.36	205	−1.71	0.36
$\frac{11}{2}$	460	−1.55	0.30	369	−1.55	0.30
$\frac{9}{2}$	0	−1.62	0.27	0	−1.49	0.27
$\frac{7}{2}$	316	−0.79	0.21	201	−1.40	0.21
$\frac{5}{2}$	96	−0.92	0.18	132	−0.35	0.17
$\frac{3}{2}$	401	0.73	0.09	379	−0.16	0.10
$\frac{1}{2}$	429		0.05	576		0.05

The $I^\pi = \frac{9}{2}^-$ state constitutes the band head of the favoured decoupled band built on the $h_{\frac{9}{2}}$ proton level at 186 and 564 keV, respectively.

TABLE 7

Calculated B(E2) ($e^2 \cdot b^2$) and B(M1) ($e^2 \cdot fm^2 \times 10^{-2}$) values and mixing ratios of the transitions between yrast states in Ir isotopes

I_i	I_f	^{187}Ir			^{189}Ir		
		B(E2)	B(M1)	δ	B(E2)	B(M1)	δ
$\frac{29}{2}$	$\frac{27}{2}$	0.02	0.03	0.15	0.09	0.03	−0.16
$\frac{29}{2}$	$\frac{25}{2}$	0.98			1.38		
$\frac{27}{2}$	$\frac{25}{2}$	0.04	0.00	−3.05	0.07	0.00	−2.90
$\frac{27}{2}$	$\frac{23}{2}$	0.95			1.13		
$\frac{25}{2}$	$\frac{23}{2}$	0.04	0.02	0.27	0.14	0.02	−0.20
$\frac{25}{2}$	$\frac{21}{2}$	0.96			1.33		
$\frac{23}{2}$	$\frac{21}{2}$	0.05	0.00	−3.33	0.08	0.00	−3.27
$\frac{23}{2}$	$\frac{19}{2}$	0.92			1.06		
$\frac{21}{2}$	$\frac{19}{2}$	0.05	0.02	0.36	0.14	0.02	−0.25
$\frac{21}{2}$	$\frac{17}{2}$	0.93			1.20		
$\frac{19}{2}$	$\frac{17}{2}$	0.07	0.00	−3.14	0.13	0.00	−3.83
$\frac{19}{2}$	$\frac{15}{2}$	0.87			0.87		
$\frac{17}{2}$	$\frac{15}{2}$	0.08	0.02	0.49	0.08	0.01	−0.24
$\frac{17}{2}$	$\frac{13}{2}$	0.89			0.99		
$\frac{15}{2}$	$\frac{13}{2}$	0.11	0.00	−2.82	0.27	0.00	−4.73
$\frac{15}{2}$	$\frac{11}{2}$	0.80			0.36		
$\frac{13}{2}$	$\frac{11}{2}$	0.14	0.02	0.75	0.07	0.01	0.36
$\frac{13}{2}$	$\frac{9}{2}$	0.82			0.82		
$\frac{11}{2}$	$\frac{9}{2}$	0.19	0.01	−2.22	0.43	0.00	−3.68

final states differ by a spin angular momentum of 2 and the single particle states are the same.

In table 10 the relative transition rates measured in these isotopes are compared with those obtained by our model. All the data are well reproduced excepting the transition rates $T(\frac{9}{2} \to \frac{11}{2})/T(\frac{9}{2} \to \frac{7}{2})$ in Au isotopes. This corresponds to the discrepancy in the excitation energies between calculated and experimental results of the $\frac{7}{2}$ state.

4.2. THE NUCLEI ^{135}Pr AND ^{133}La

These nuclei are situated in the new deformation region in which the second 2^+ state lies around the first 4^+ state; and the second 0^+ state appears at higher energies. Recently Habs *et al.* [13]) studied extensively the nuclei in the region $50 < (N, Z) < 82$ using the anharmonic vibrator model of Greiner and Gneuss [14]). They found for the nuclei around $A = 135$, triaxial shapes and energy minimum at asymmetries of about $\gamma = 30°$ indicating the presence of γ-deformation in these nuclei. Our calculations for ^{135}Pr and ^{133}La give $\gamma = 24.7°$ for ^{135}Pr and $\gamma = 25.5°$ for ^{133}La in good agreement with calculations of Habs *et al.* The measured high-spin states [15])

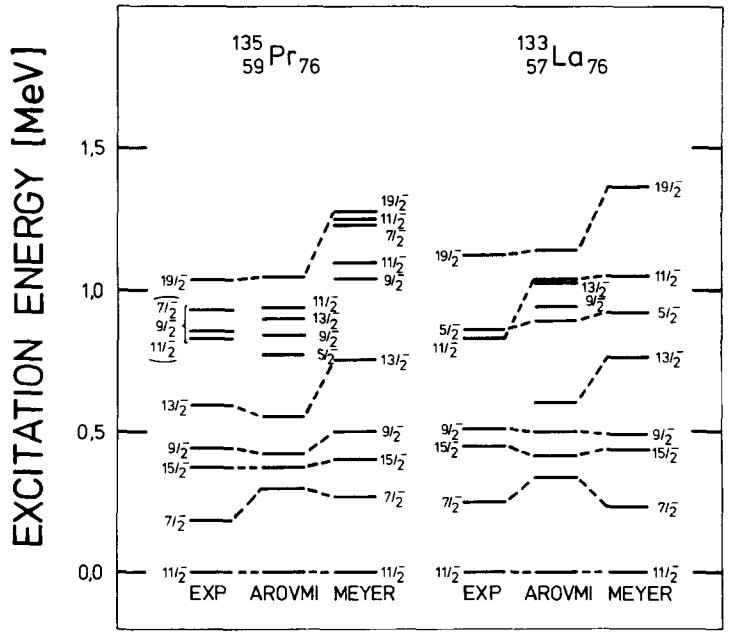

Fig. 4. Experimental and calculated excitation energies of decoupled bands built on a $h_{\frac{11}{2}}$ proton of ^{135}Pr and ^{133}La. Abbreviations used are explained in fig. 1. Parameters used in our calculations are (i) $\beta = 0.215$, $\gamma = 24.7°$, $\lambda = -1.76$ MeV, $\theta_{00}/\hbar^2 = 9.81$ MeV^{-1}, $C = 0.0330$ MeV^3 for ^{135}Pr, (ii) $\beta = 0.210$, $\gamma = 25.4°$, $\lambda = -1.82$ MeV, $\theta_{00}/\hbar^2 = 8.88$ MeV^{-1}, $C = 0.0373$ MeV^3 for ^{133}La. The ground-state rotational energies of the core are taken from experiment (see fig. 1 caption).

TABLE 8

Calculated excitation energies (keV) relative to the $I^\pi = \frac{11}{2}^-$ state, quadrupole moments ($e \cdot b$) and magnetic moments ($e \cdot fm$) of yrast states in ^{135}Pr and ^{133}La

I	^{135}Pr			^{133}La		
	E	Q	μ	E	Q	μ
$\frac{19}{2}$	1045	−0.92	0.97	1143	−0.92	0.96
$\frac{17}{2}$	1036	−1.14	0.89	1116	−1.11	0.89
$\frac{15}{2}$	376	−1.49	0.88	412	−1.46	0.88
$\frac{13}{2}$	552	−0.98	0.78	601	−0.95	0.78
$\frac{11}{2}$	0	−1.40	0.78	0	−1.36	0.78
$\frac{9}{2}$	419	−1.33	0.56	497	−1.17	0.66
$\frac{7}{2}$	302	−0.73	0.66	338	−0.79	0.66
$\frac{5}{2}$	771	−0.82	0.49	893	−0.76	0.49
$\frac{3}{2}$	1048	−0.13	0.46	1151	−1.49	0.46
$\frac{1}{2}$	1692		0.00	1856		−0.02

The $I^\pi = \frac{11}{2}^-$ state constitutes the band head of the favoured decoupled band built on the $h_{\frac{11}{2}}$ neutron level at 358 and 536 keV, respectively.

TABLE 9

Calculated B(E2) ($e^2 \cdot b^2$) and B(M1) ($e^2 \cdot fm^2 \times 10^{-2}$) values and mixing ratios of the transitions between yrast states in ^{135}Pr and ^{133}La

I_i	I_f	^{135}Pr			^{133}La		
		B(E2)	B(M1)	δ	B(E2)	B(M1)	δ
$\frac{19}{2}$	$\frac{17}{2}$	0.08	0.51	0.00	0.07	0.55	0.00
$\frac{19}{2}$	$\frac{15}{2}$	0.46			0.39		
$\frac{17}{2}$	$\frac{15}{2}$	0.20	0.14	−0.69	0.18	0.16	−0.65
$\frac{17}{2}$	$\frac{13}{2}$	0.27			0.25		
$\frac{15}{2}$	$\frac{13}{2}$	0.00	0.36	0.01	0.00	0.37	0.01
$\frac{15}{2}$	$\frac{11}{2}$	0.37			0.31		
$\frac{13}{2}$	$\frac{11}{2}$	0.31	0.19	−0.62	0.27	0.22	−0.59

built on a $h_{\frac{11}{2}}$ proton for these two nuclei are compared with our calculations as well as with those of Meyer-ter-Vehn and are shown in fig. 4. It is evident from fig. 4 that our model can reproduce the data generally better, especially for the higher-spin states. The calculated excitation energies, different moments and transitions are listed in tables 8 and 9. As discussed for the nuclei in the Au region, one can also see the same regularities for the B(E2) and B(M1) values and the mixing ratios δ. The relative transition rates measured in ^{135}Pr and ^{133}La are compared with our model calculation in table 10.

It is interesting to study the overlap $\langle IMR\alpha j|IM\rangle$ of the exact wave function $|IM\rangle$ with the functions (7) which have a good core angular momentum. This yields information about the nature of the low-spin states. Again one finds that for the

TABLE 10

Experimental and calculated relative transition rates

Nucleus	I_i	$E_i \to I_f$ (keV)	E_f (keV)	Relative transition rates exp	theory
^{191}Hg	$\frac{19}{2}$	$1172 \to \frac{15}{2}$	535	57	23
		$\frac{17}{2}$	390	100	100
^{193}Hg	$\frac{19}{2}$	$1240 \to \frac{15}{2}$	606	71	19
		$\frac{17}{2}$	382	100	100
^{193}Au	$\frac{9}{2}$	$601 \to \frac{7}{2}$	218	100	100
		$\frac{11}{2}$	0	18	226
^{195}Au	$\frac{9}{2}$	$575 \to \frac{7}{2}$	207	100	100
		$\frac{11}{2}$	0	59	413
^{195}Au	$\frac{11}{2}$	$962 \to \frac{9}{2}$	575	100	100
		$\frac{13}{2}$	560	6	75
		$\frac{7}{2}$	207	20	10
		$\frac{11}{2}$	0	65	45
^{187}Ir	$\frac{11}{2}$	$434 \to \frac{13}{2}$	164	12	18
		$\frac{9}{2}$	0	100	100
^{187}Ir	$\frac{15}{2}$	$715 \to \frac{17}{2}$	489	16	6
		$\frac{11}{2}$	434	24	27
		$\frac{13}{2}$	164	100	100
^{187}Ir	$\frac{19}{2}$	$1131 \to \frac{21}{2}$	953	16	3
		$\frac{15}{2}$	715	21	107
		$\frac{17}{2}$	489	100	100
^{187}Ir	$\frac{23}{2}$	$1661 \to \frac{19}{2}$	1131	100	100
		$\frac{21}{2}$	953	38	42
^{135}Pr	$\frac{9}{2}$	$441 \to \frac{7}{2}$	185	18	3
		$\frac{11}{2}$	0	100	100
^{133}La	$\frac{9}{2}$	$510 \to \frac{7}{2}$	249	14	5
		$\frac{11}{2}$	0	100	100

Experimental energies relative to the lowest $I = j$ state of each nucleus specify the initial and the final states.

TABLE 11

Nature of the low-spin states $|IM\rangle$

I	^{195}Hg				^{195}Au				^{135}Pr			
	R	(N)	$j = \frac{13}{2}$	A^2(%)	R	(N)	$j = \frac{11}{2}$	A^2(%)	R	(N)	$j = \frac{11}{2}$	A^2(%)
$\frac{1}{2}$	6	0	=	95.7	6	0	$\neq$	79.2	6	0	$\neq$	57.3
$\frac{3}{2}$	6	0	$\neq$	95.2	4	0	=	77.9	4	0	=	89.1
$\frac{5}{2}$	4	0	=	95.4	4	0	$\neq$	75.3	4	0	$\neq$	68.5
$\frac{7}{2}$	4	0	$\neq$	90.8	2	0	=	77.6	2	0	=	87.6
$\frac{9}{2}$	2	0	=	91.0	2	0	$\neq$	56.7	2	0	$\neq$	59.9
$\frac{11}{2}$	2	0	$\neq$	67.3	0	0	=	56.6	0	0	=	65.2

The square of the amplitude $A = \langle IMR\alpha j|IM\rangle$ (eq. (12a)] is given. Here I is the total angular momentum and R the angular momentum of the core. The projection N of R to the intrinsic z-axis is only approximately a good quantum number and N may characterize the different core states α for the same spin R. The symbol "=" indicates that the single particle angular momentum j is antiparallel to the core angular momentum R. The symbol "$\neq$" indicates that the direction of j is tilted against the direction of R. The core angular momentum R stands always perpendicular to the intrinsic z-axis for the main admixture.

favoured angular momenta ($j-I$ = even) the main component of the wave function has the core angular momentum R (anti)parallel to the single particle angular momentum j (see table 11). For the unfavoured angular momenta ($j-I$ = odd) one still finds that R is perpendicular to the intrinsic z-axis, but the single particle angular momentum is not antiparallel. It is tilted against the direction of R (see table 11).

5. Discussion

It has been shown that the decoupled bands in the odd-mass nuclei in the transitional regions are reproduced by the model based on an odd quasi-particle coupled to an asymmetric rotor with a variable moment of inertia. Our model in which we take into account the softness of the core improves especially the fit to the higher-spin states for which Meyer-ter-Vehn [3, 12]) finds considerable deviation from experiments. Besides, our treatment in which we expand the basis states in terms of the core eigenstates has a desired feature that we can use the experimental excitation energies for the core instead of the predicted values of the VMI model in order to include all effects of the core. This is very remarkable for the calculation of the anomaly of the rotational spectrum of Hg isotopes. As for the lower-spin states, however, inclusion of the softness of the core does not improve the results given by the rigid asymmetric rotor model. It is a further problem of the asymmetric rotor model that the lower-spin states are always higher than the experiments. It may be remedied by considering additional single particle levels not included in our model.

Our calculations in which we use the minimization procedure to fix the parameters give almost same values for the γ-deformation as those used by Meyer-ter-Vehn [3, 12]) and yield in these transitional nuclei (A = 190 and A = 135) rather stable triaxial shapes (apart from the Ir isotopes). This contradicts calculations of the β, γ deformation energy surface [16]) which predict γ-soft nuclei with minima at positive ($\gamma = 0°$) or negative ($\gamma = 60°$) deformations. However, recently Habs *et al.* [13]) found pronounced minima for the nuclei around A = 135 in the empirical potential energy surface using the anharmonic vibrator model of Greiner and Gneuss [14]). Their results of γ-deformation value are very similar to our values. These results suggest that these transitional nuclei have rather well defined γ-deformations. This seems to be a challenge for further theoretical studies of the deformation energy surface which are not able at present to produce such well defined minima in the γ-direction.

References

1) F. S. Stephens, R. M. Diamond, J. R. Leigh, T. Kammuri and K. Nakai, Phys. Rev. Lett. **29** (1972) 438;
P. O. Tjøm, M. R. Maier, D. Benson, Jr., F. S. Stephens and R. M. Diamond, preprint LBL-2379 (1974);
S. André, J. Boutet, J. Rivier, J. Trehence, J. Jastrzebski, J. Lukasiak, Z. Sujkowski and C. Sebille-Schück, preprint;
R. M. Lieder, H. Beuscher, W. F. Davidson, A. Neskakis and C. Mayer-Böricke, preprint

2) F. S. Stephens, R. M. Diamond, D. Benson, Jr., and M. R. Maier, Phys. Rev. **C7** (1973) 2163; F. S. Stephens, Proc. of the Int. Conf. on nuclear physics, Munich (1973)
3) J. Meyer-ter-Vehn, F. S. Stephens and R. M. Diamond, preprint LBL-2394; J. Meyer-ter-Vehn, preprint LBL-3416
4) M. A. J. Mariscotti, G. S. Goldhaber and B. Buck, Phys. Rev. **178** (1969) 1864
5) J. A. Nelder and R. Nead, Computer J. **7** (1965) 308
6) A. Bohr, Mat. Fys. Medd. Dan. Vid. Selsk. **26** (1952) 14
7) A. S. Davydov and G. F. Filippov, Nucl. Phys. **8** (1958) 237
8) A. Faessler, W. Greiner and R. K. Sheline, Nucl. Phys. **70** (1965) 33
9) K. S. Krane and R. M. Steffen, Phys. Rev. **C2** (1970) 724
10) A. Bohr and B. R. Mottelson, Nuclear structure, vol. 1 (Benjamin, New York, 1969)
11) L. Grodzins, Phys. Lett. **2** (1962) 88
12) J. Meyer-ter-Vehn, preprint LBL
13) D. Habs, H. Klewe-Nebenius, K. Wisshak, R. Löhken, G. Nowicki and H. Rebel, Z. Phys. **267** (1974) 149
14) G. Gneuss and W. Greiner, Nucl. Phys. **A171** (1971) 449
15) R. A. Meyer, preprint UCRL-76207
16) K. Kumar and M. Baranger, Nucl. Phys. **110** (1968) 529; **A126** (1969) 15